ISIJ International, Vol. 56 (2016), No. 9, pp. 1598–1605

Optimization of the Dehydration Temperature of Goethite to Control Pore Morphology

Genki SAITO,* Takahiro NOMURA, Norihito SAKAGUCHI and Tomohiro AKIYAMA

Center for Advanced Research of Energy and Materials, Hokkaido University, Sapporo, 060-8628 Japan.

(*Received on April 20, 2016; accepted on June 7, 2016*)

This study optimizes the dehydration temperature of goethite to control pore morphology. The pore morphology was characterized by using transmission electron microscopy and the nitrogen adsorption method. When the goethite was dehydrated at 200–250°C, slit-like pores with a width lesser than 2 nm were formed along the [010] direction. These slit-like pores changed to spherical micropores (300–500°C), and eventually disappeared (600–800°C). Compared to the synthetic goethite, natural goethite has a lower crystallinity and smaller primary particle size of under 100 nm. The natural goethite before dehydration contained 4 nm pores as cracks that remained even after heating to 800°C. In the case of natural goethite, the optimum dehydration temperature for higher surface area and pore volume was 350°C, which was higher than that of 250°C for the synthetic goethite.

KEY WORDS: dehydration temperature; pore morphology; goethite.

1. Introduction

Goethite (αFeOOH), one of the thermodynamically stable iron oxides, is widely distributed in soils, rocks, sediments, and ores.[1,2] Goethite and hematite (αFe_2O_3) obtained by goethite decomposition have been used as pigments,[2] water purification catalysts,[3] magnetic materials,[4] and iron making resources.[5–20] Recently, composite materials of iron ore and carbon have been fabricated for enhancing the reduction rate of iron oxide.[6,7] Chemical vapor infiltration (CVI) has been applied for preparing such composite materials, in which the tar-containing gas is generated by the pyrolysis of carbonaceous resources that are deposited into nano-sized pores produced by the decomposition of goethite.[5,10,14] Therefore, understanding pore generation during goethite decomposition becomes much more important.

Numerous articles related to study of the goethite-hematite phase transformation by thermogravimetric analysis,[21–26] pore morphology observation,[22,27–32] crystal structure analysis,[22,23,29,31–34] and using substitutional elements such as Al and Ti[35–37] have been published. When goethite transforms to hematite by thermal decomposition at lower temperature (below 300°C), uniform slit-shaped micropores are formed in the hematite.[31] With increasing temperature, these micropores grow to form coarse pores. Electron microscopy and X-ray diffraction studies have confirmed the direct transformation of goethite to hematite without any intermediate phases.[26,30] Although these studies have clarified the phase transformation mechanism, the optimum dehydration temperature to fabricate a porous structure with high surface area and pore volume is still unclear, despite the importance of these parameters for applications. In particular, the pore evolution of natural goethite is not well understood. To utilize goethite as a tar decomposition catalyst and an iron-making resource, a method to control pore morphology is essential. Therefore, this study optimizes the dehydration temperature of goethite to control pore morphology, in which the effect of dehydration temperature ranging from 100 to 800°C on the pore morphology was studied using thermogravimetric analysis (TG), X-ray diffraction (XRD), nitrogen adsorption, and transmission electron microscopy (TEM). We compared synthetic and natural goethite for use as starting materials. In general, natural goethite contains impurities, which might affect the dehydration behavior. Finally, we determine the optimum dehydration temperature required to obtain higher surface area and pore volume of the synthetic and natural goethite.

2. Experiment

Synthetic rod-like goethite powder (99% purity, Kojundo Chemical Lab. Co.) with a particle size of 1 μm and natural goethite ore (CaO: 0.05 mass%, SiO_2: 4.53 mass%, Al_2O_3: 1.55 mass%) with 2–3 mm grain size[12] and a primary particle size of less than 100 nm were used as starting materials. These particles were vacuum dried at 100°C for 24 h. The dehydration behavior of these samples was investigated using a thermogravimetric analyzer (TG-DSC, Mettler Toledo). For TG analysis, an alumina sample pan containing 10 mg of the sample was used in an air atmosphere with a flow rate of 100 mL/min; the temperature was increased from 25 to 800°C at a rate of 10°C/min. Since the detailed characterization requires a significant amount of powder, an electronic furnace was used for dehydration of a 6 g sample. In the case of holding temperatures of

* Corresponding author: E-mail: genki@eng.hokudai.ac.jp
DOI: http://dx.doi.org/10.2355/isijinternational.ISIJINT-2016-231

230, 250, 300 and 350°C, the dehydration time was 24 h, and the holding time was 1 h over 500°C. Powder X-ray diffraction (XRD, Rigaku Miniflex II, Cu-kα) was used to characterize the phase composition. The Brunauer-Emmett-Teller (BET) specific surface area,[38] total pore volume, and Barrett-Joyner-Halenda (BJH) pore size distribution analysis of samples were characterized by nitrogen adsorption using Autosorb 6AG (Quantachrome instruments). Before measurement, samples were pre-heated at 120°C for 4 hours under vacuum. A total of 79 points, including adsorption and desorption, were obtained across a relative pressure range (P/P_0) from 0.025 to 1.00 at 77 K. The pore morphology was characterized by using a 200 kV transmission electron microscope (TEM, JEOL, JEM-2010F). Ethanol droplets, containing sample powders in suspension, were placed onto a collodion-coated Cu microgrid (150 mesh, Nisshin EM), and subsequently dried at 60°C in an oven before TEM observation. A 300 kV TEM (FEI Titan) was employed for TEM tomography analysis using the tomography holder with a tilt range of ±60°. Amira software was used to create 3D images.

3. Results and Discussions

3.1. Dehydration Behavior

Figure 1 shows the differential thermal analysis (DTA) and differential scanning calorimetry (DSC) curves during thermal decomposition of the samples. Both the synthetic and natural goethite showed approximately 10% weight loss after dehydration, which is due to the transformation of goethite to hematite, as shown in Eq. (1).

$$2FeOOH \rightarrow Fe_2O_3 + H_2O \quad \text{..... (1)}$$

Theoretically, a weight loss of 10.13% is predicted according to Eq. (1); this value is in agreement with the observed weight loss. The endothermic heat of the synthetic and natural goethite was 290 and 303 J/g, respectively; the theoretical endothermic heat, as predicted by Eq. (1), at 280°C was 291.5 J/g, which was calculated using the initial weight of FeOOH. Based on the assumption of H_2O evaporation, the theoretical endothermic heat was determined to be 2 877 J/g (H_2O basis), which is higher than the theoretical evaporative latent heat of H_2O at 100°C (2 260 J/g). The increased evaporative latent heat was caused by the ridge bonding structure of combined water. From these results, it is evident that the synthetic and natural goethite contained a similar amount of combined water. However, the derivative of weight and change in heat flow showed different characteristics for each sample. In the case of the natural goethite, a broad peak at 274°C was observed. In contrast, two peaks at 249°C and 284°C appeared in the curve for the synthetic goethite curve. This difference can be explained by the crystallinity according to the report of Schwertmann.[39] This report attributed the appearance of a peak at reduced temperature to the impairment of crystallinity. With a sample of lower crystallinity, such as natural goethite, this peak will not be clearly visible. However, high crystallinity results in the change in unit cell size and occurs at a higher temperature. Compared to the natural goethite, the synthetic goethite has a higher crystallinity, and consequently, the dehydroxylation peak splits into two peaks. In contrast, natural goethite has low crystallinity with a primary particle size of less than 100 nm, which caused the natural goethite to dehydrate at a lower temperature than the synthetic goethite. Weight loss of natural goethite was observed for temperatures even beyond 300°C. Liu *et al.* reported that natural goethite

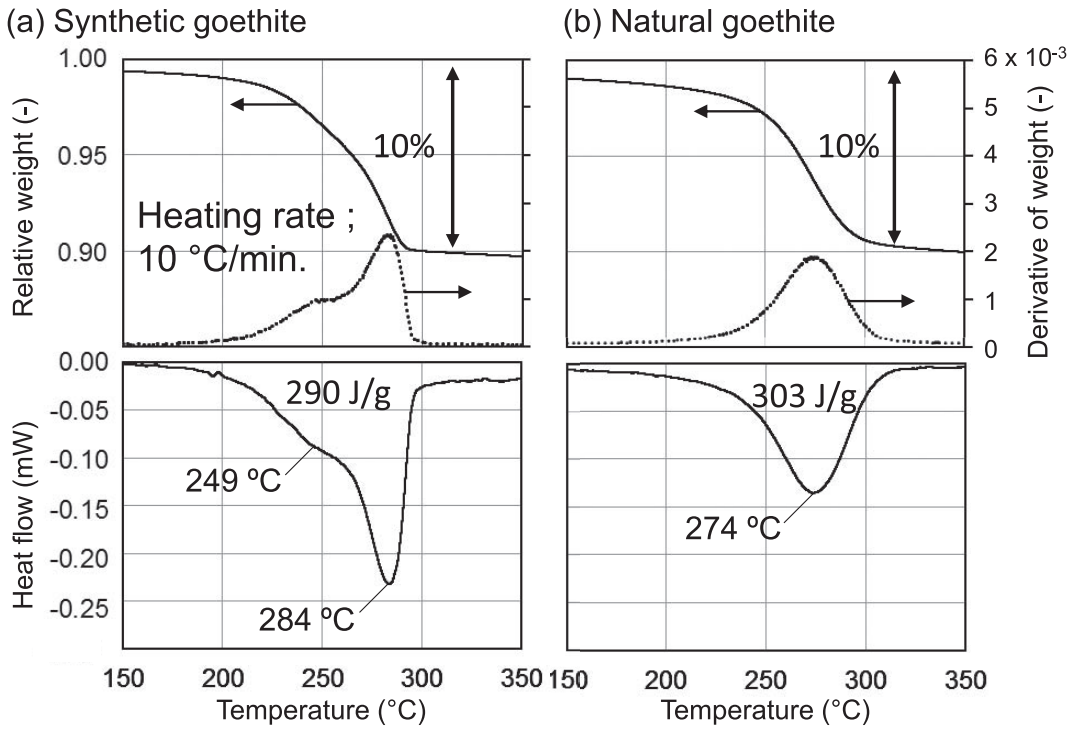

Fig. 1. DTA and DSC curves during the dehydration of (a) synthetic goethite and (b) natural goethite, in which the dashed line shows the derivative of weight. Both synthetic and natural goethite showed 10% weight loss after dehydration. The endothermic heat of the synthetic and natural goethite were 290 and 303 J/g, respectively.

contains non-stoichiometric OH units, and that combined water in this form still existed in the goethite after heating at 800°C.[22] From these results, it is suggested natural goethite can contain much more combined water compared to synthetic goethite.

Based on the DTA and DSC analysis, the dehydration temperature was varied from 200 to 800°C. Since the complete dehydration required a long time at a temperature less than 300°C, the synthetic and natural goethite were kept for 24 hours in an electric furnace. **Figure 2** shows the XRD patterns of samples after heat treatment at different conditions with the crystal definitions: a_G = 0.996 nm, b_G = 0.302 nm, and c_G = 0.462 nm for goethite, and a_H = b_H = 0.504 nm and c_H = 1.377 nm for hematite. In the case of the synthetic goethite, the transformation of goethite occurred at a temperature greater than 250°C, and the peak became sharper with increase in temperature, which is attributed to crystal growth. The change in peak intensity ratio of $(104)_H$ and $(110)_H$ might have been caused by the crystal orientation because the synthetic goethite has a rod-like morphology in the growth direction of $[010]_G$. Compared to the synthetic goethite, the natural goethite had a lower crystallinity and lower decomposition temperature of 230°C. After the transformation of the natural goethite to hematite, the sharpness of the peak did not change significantly; this indicated that there was no notable crystal growth or sintering of primary particles as in the synthetic goethite. The difference between the synthetic and natural goethite might be caused by the particle structure and pore morphology, which affects crystal growth. Therefore, further analysis was performed by nitrogen adsorption and TEM observation.

3.2. Adsorption Analysis

The nitrogen adsorption method is widely used for the analysis of surface area and porous morphologies. **Figure 3** shows the nitrogen adsorption-desorption isotherms of synthetic and natural goethite. In the case of synthetic goethite dehydrated at 250°C, the amount of adsorption was increased at the lower range of relative pressure in comparison with the curve before dehydration, shown in Fig. 3(a). This result reveals the increase in the number of micropores with pore size of less than 2 nm after dehydration at 250°C, because the amount of adsorption at a relative pressure below 0.1 corresponds to micropore filling. After dehydration at 500°C, the number of micropores was reduced and hysteresis was observed at $P/P_O > 0.4$ between adsorption and desorption. In general, hysteresis of adsorption-desorption isotherms is caused by capillary condensation of adsorbent into mesopores (2–50 nm). According to the classification by De Boer,[40] the obtained isotherm shown in Fig. 3(c) is attributed to slit-like mesopores. At 800°C, the amount of adsorption was significantly decreased, which might be indicative of the disappearance of pores and agglomeration in particles. In contrast to the synthetic goethite, the as-received natural goethite demonstrates hysteresis of the nitrogen adsorption-desorption isotherms more clearly, which suggests the original existence of mesopores in the natural goethite. Similar to the case of synthetic goethite, the number of micropores was increased by dehydration at 250°C and mesopores developed at 500°C owing to pore growth. Hysteresis appeared until 800°C, which indicated the presence of remaining mesopores. In summary, natural goethite originally contained slit-like mesopores, which remained after heating at 800°C.

To evaluate the surface area, the BET method was used as described by the following equation (Eq. (2)).

$$\frac{1}{W\left(\left(P_O / P\right)-1\right)} = \frac{1}{W_m C} + \frac{C-1}{W_m C}\left(\frac{P}{P_O}\right) \quad \text{..... (2)}$$

Here, W indicates the weight of gas adsorbed, P/P_O corresponds to the relative pressure, W_m is the weight of adsor-

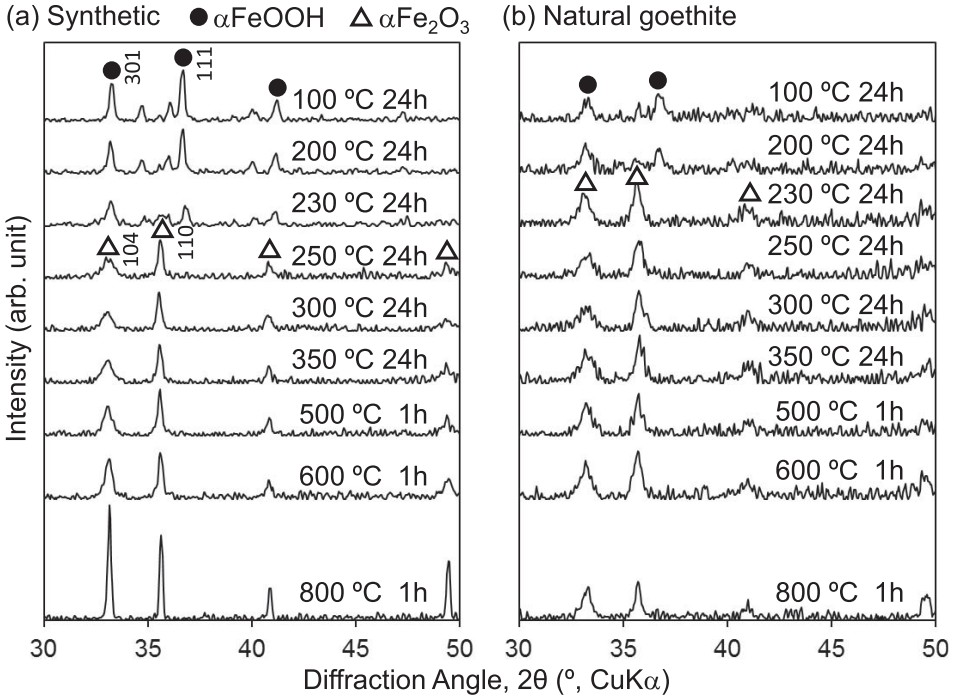

Fig. 2. XRD patterns of the samples after heat treatment at different temperatures.

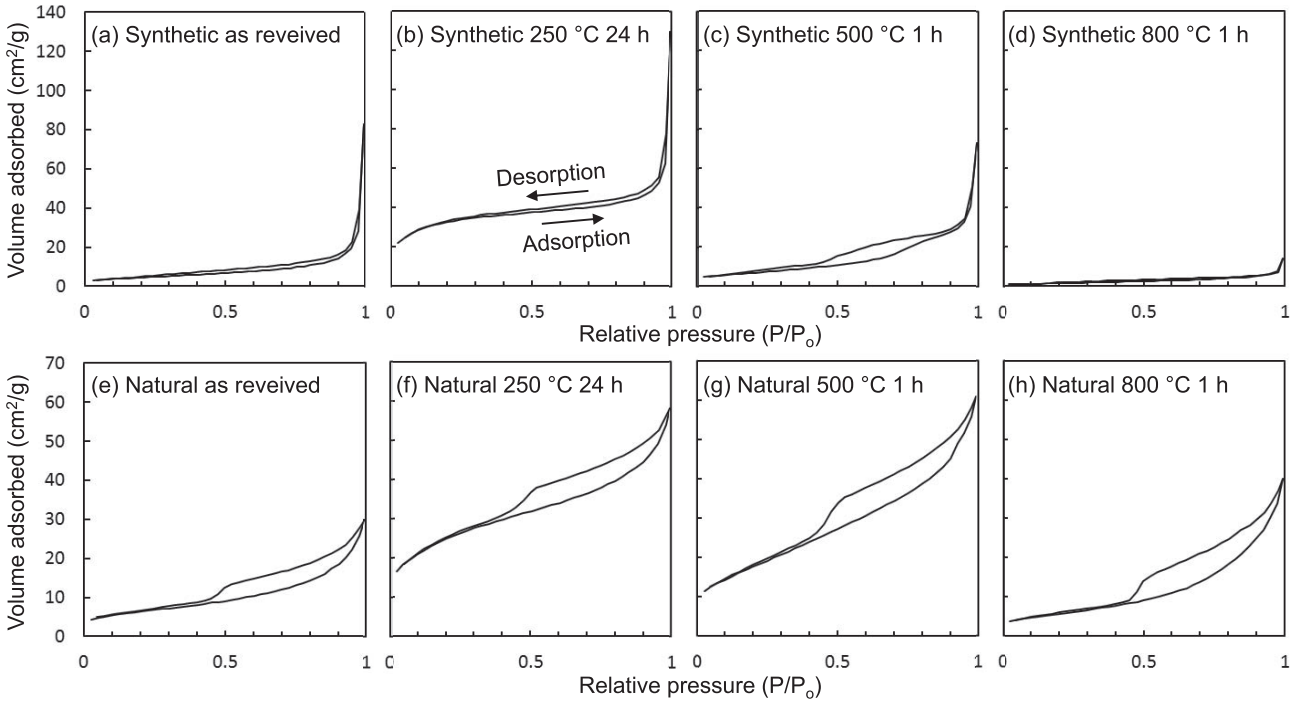

Fig. 3. Nitrogen adsorption-desorption isotherms of synthetic and natural goethite under different dehydration conditions.

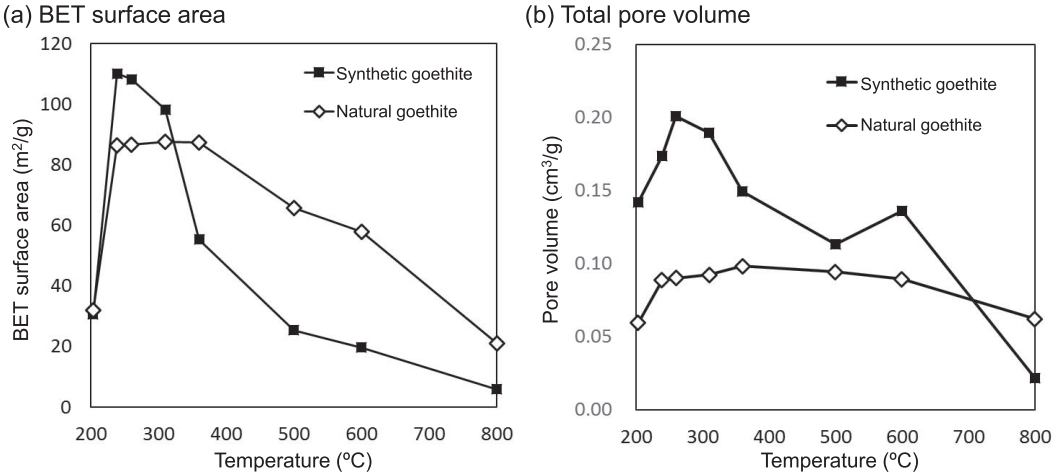

Fig. 4. Summary for heating temperature dependence of the (a) BET surface area and (b) total pore volume, which were calculated from the nitrogen isotherm plots. The crystal structure of each sample was confirmed by XRD, as shown in Fig. 2. The BET surface area and pore volume before heat treatment were 16.4 m^2/g and 0.13 cm^3/g in the synthetic goethite, and 21.7 m^2/g and 0.05 cm^3/g in the natural goethite, respectively.

bate as a monolayer, and C is the BET constant. The multipoint BET plots were obtained with P/P_O ranging from 0.05 to 0.35 and had a good linearity. **Figure 4** summarizes the heating temperature dependence of the (a) BET surface area and (b) total pore volume, which was calculated from the nitrogen isotherm plots. Total pore volume was calculated based on the total gas volume at $P/P_O \approx 1$. The BET surface area and pore volume before heat treatment were 16.4 m^2/g and 0.13 cm^3/g in the synthetic goethite, and 21.7 m^2/g and 0.05 cm^3/g in the natural goethite, respectively. The surface area of the synthetic goethite showed a marked increase to 110 m^2/g at 230°C and then decreased to 25.4 m^2/g at 500°C. The pore size distribution was analyzed by the BJH method, which is an established method for pore size analysis based on the cylindrical pores model. In this method, capillary condensation in the pores was calculated based on the Kelvin-type equation shown below (Eq. (3)).

$$r_K = \frac{-2\gamma V_m}{RT \ln(P / P_O)} \quad \text{..... (3)}$$

Here, r_K is pore radius, γ and V_m are surface tension and the molar volume of nitrogen, respectively, R is the gas constant, and T is the absolute temperature. **Figure 5** shows the pore size distribution for the as-heated sample calculated from the adsorption–desorption curve using BJH analysis. In the case of the synthetic goethite, the small pores with a pore size of less than 2 nm were formed at temperatures ranging from 230 to 250°C, resulting in an increase of the surface area. With increasing temperature, the pores grew larger and then disappeared after the temperature increased

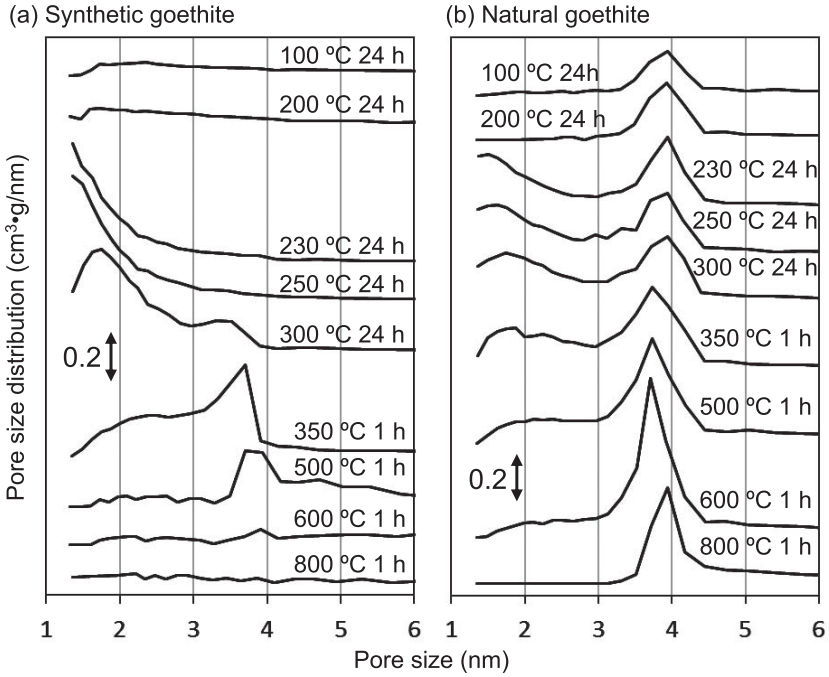

Fig. 5. Pore size distribution calculated from the absorption-desorption curve for the as-heated samples.

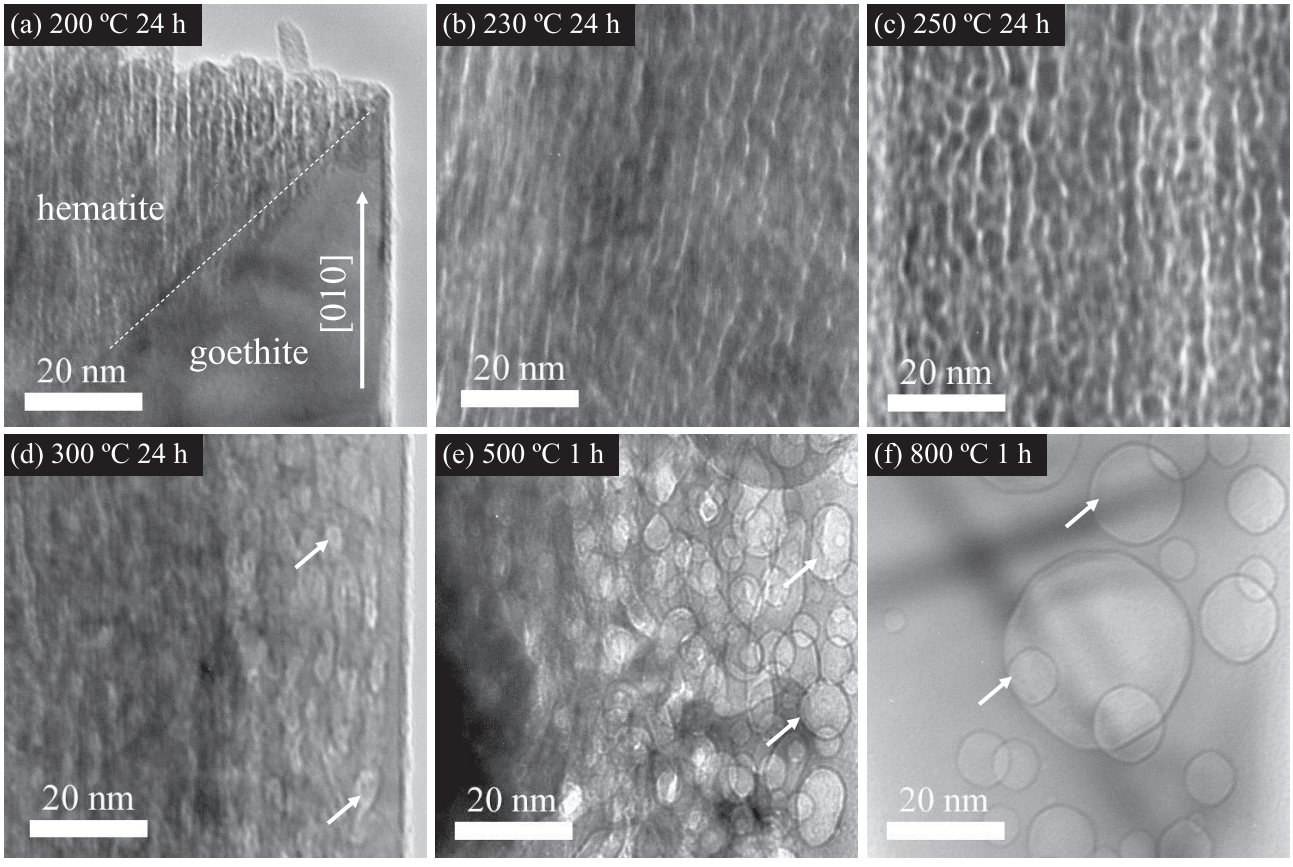

Fig. 6. TEM images of synthetic goethite powders after heat treatment at different temperatures. Arrows show the micropores and cratered surface.

beyond 600°C owing to pore growth. In contrast, the BET surface area of the natural goethite was found to be about 86–87 m^2/g from 230 to 350°C, and the surface area gradually decreased at higher temperatures. From the pore size distribution shown in Fig. 5(b), it can be seen that the original natural goethite (before thermal decomposition) contained 4 nm pores; these pores remained even at 800°C. In the temperature range from 230 to 300°C, the small pores with a size lesser than 2 nm were also observed, similar to those in the synthetic goethite. Owing to the existence of 4 nm pores, the natural goethite had a higher surface area than the synthetic goethite at higher temperatures over 300°C than the synthetic goethite. Kashiwaya *et al.* reported the formation of 4 nm cracks generated into the natural goe-

thite particle, in which cross-sectional sample was prepared using focused ion beam.[27] Therefore, the 4 nm pores in the original natural goethite (Fig. 5(b)) are understood to be cracks. When the dehydration temperature was 350°C, both synthetic and natural goethite mainly contained 4 nm pores. However, the pore structure is considered to be different between synthetic and natural goethite. For further investigation, the TEM observation was carried out described at section 3.3. In contrast to the decreasing rate of pore volume change in the synthetic goethite, the pore volume change in the natural goethite was relatively moderate because of the existence of 4 nm pores. In summary, the decomposed synthetic goethite had a high BET surface area of 108 m^2/g and pore volume of 0.2 cm^3/g at 250°C. The pores generated in the synthetic goethite grew easily at high temperatures over 300°C. Compared to the synthetic goethite, the change in BET surface area and total pore volume of the natural goethite was relatively mild due to the presence of 4 nm pores. The optimum dehydration temperature for higher surface area and larger pore volume was 350°C for the natural goethite, where it had a surface area of 87 m^2/g and pore volume of 0.1 cm^3/g.

3.3. TEM Observation of Pore Morphology

To study the pore morphologies at each temperature, the samples were observed by TEM. **Figure 6** shows the TEM images of synthetic goethite powders after heat treatment. The synthetic goethite powder had a rod-like shape with a growth direction of [010]. At 200°C, the tip of the rod was partially dehydrated to hematite with the slit-like pores generation in the [010] direction of the original goethite in Fig. 6(a). When the goethite was dehydrated at 230–250°C, the slit-like pores with a width lesser than 2 nm were formed over the entire area of the rod in the [010] direction, with simultaneous transformation from goethite to hematite, as indicated by the XRD patterns shown in Fig. 2. Similar slit-like pore generation was reported by Naono *et al.*[29,31] and Walter *et al.*[25] The observed change in the slit width is in good agreement with the pore size distribution shown in Fig. 5(a). According to the atomic structure model shown in **Fig. 7**, the OH groups were closely arranged in the goethite [010] direction, resulting in the formation of slit-like pores in the [010] direction. When the temperature was in the range of 300–500°C, the transformation to hematite was almost completed and the slit-like pores changed to spherical micropores (see arrows) because of crystal growth. Eventually, the pores almost disappeared, leaving behind a cratered surface (see arrows) at 800°C. For three-dimensional (3D) analysis of pore generation, TEM tomography was performed, where the sample was observed at the different angles ranging from −60 to 60°. **Figure 8**(a) shows the 3D-reconstructed image of the synthetic goethite rod-shaped powder dehydrated at 300°C. From the virtually sliced images shown in Figs. 8(b)–8(d), it can be seen that the pores were uniformly located in the synthetic goethite rod. **Figure 9** is a schematic diagram of the pore morphology evolution of the synthetic goethite at elevated temperature.

The natural goethite was also observed by TEM, where the natural goethite was crushed for TEM sample preparation. As shown in **Fig. 10**(a), the original ore (before thermal decomposition) was an aggregate consisting of small primary particles less than 100 nm in size. This result was in agreement with the XRD analysis shown in Fig. 2(b). No pores were observed in the particles before thermal decomposition. The 4 nm pores in the original natural goethite might existed as cracks. During crushing of particles, the pulverization occurred through these cracks. Thus, the 4 nm cracks were not clearly observed by TEM. When the natural goethite was heated to 230°C, slit-like pores were generated in the particles (see the arrows in Fig. 10(b)). Similar to the case of synthetic goethite, these slit-like pores might be generated because of the removal of OH. With increasing temperature, the pores in the particles grew to a spherical shape, and the outer surface of the particle became smooth and rounded. However, the particle size did not change since the particles did not undergo sintering. This result also explained the reason for lower crystallinity at high temperature (Fig. 2(b)). In the synthetic goethite, the single-crystalline goethite with a particle size of 1 μm initially transformed to the polycrystalline hematite, and then crystal growth occurred to transform it to a nearly single-crystalline hematite particle at an elevated temperature from 300 to 800°C. Unlike the synthetic goethite, the primary particles of the natural goethite were very small, with a size less than 100 nm, and the crystal growth occurred only in the primary particles. In addition, impurities might affect the dehydration and sintering behavior. In particular, Al and Ti ions can substitute on the Fe site.[35–37] From these results, it is found that the initial state, *e.g.*, pre-existing cracks, and impurities

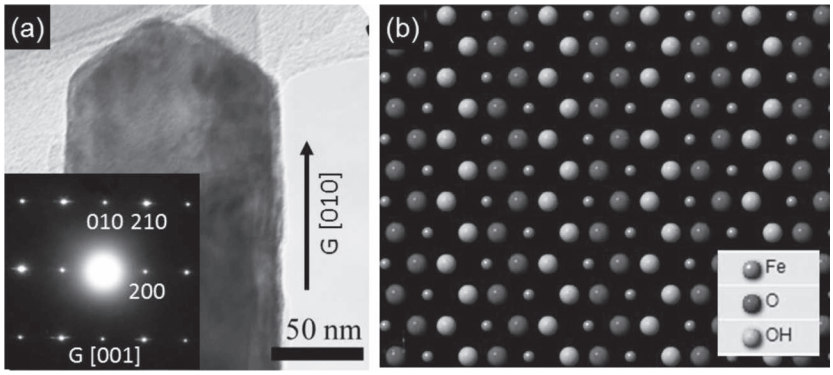

Fig. 7. (a) TEM image and corresponding electron diffraction pattern of the synthetic goethite rod. (b) Atomic structure model corresponding to the goethite in Fig. 6(a).

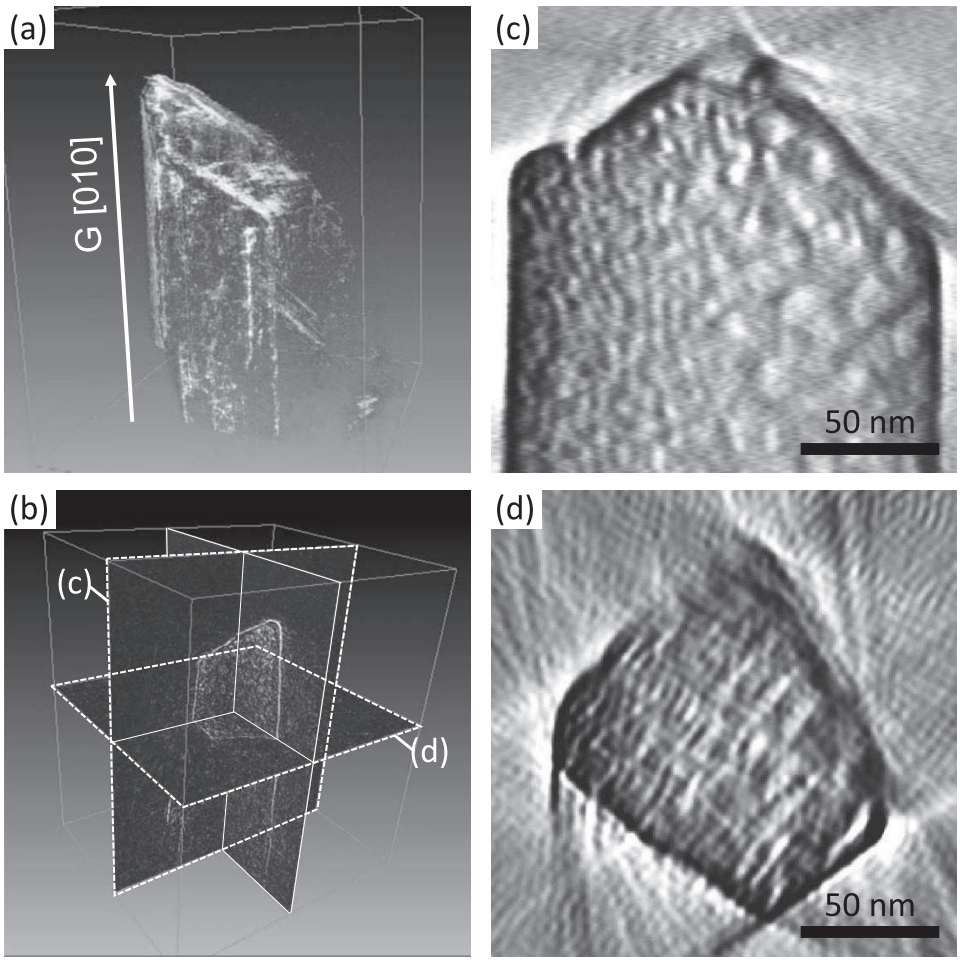

Fig. 8. (a) Three-dimensionally reconstructed image obtained by TEM tomography for the synthetic goethite powder dehydrated at 300°C. (b) Virtual slices along the X, Y, and Z-axis. (c, d) 2-D image of the virtual slices corresponding to (b).

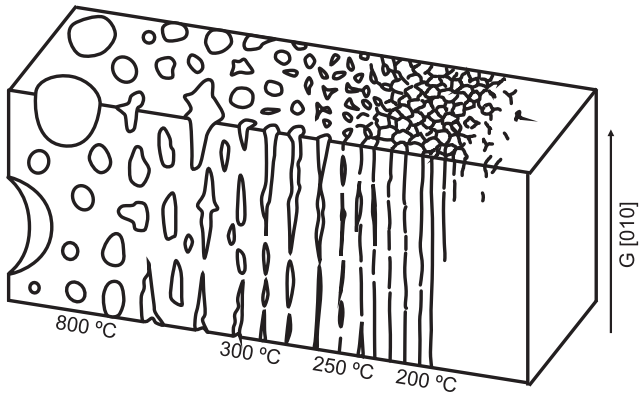

Fig. 9. Schematic diagram of pore morphology evolution at elevated temperature.

of the goethite can also affect the generation of pores.

4. Conclusion

This study investigates the effect of dehydration temperature, ranging from 100 to 800°C, on the pore morphology of the synthetic and natural goethite. The following conclusions were drawn:

(1) When the synthetic goethite was dehydrated at 200–250°C, slit-like pores with a width less than 2 nm were formed in the goethite [010] direction. These slit-like pores changed to spherical micropores (300–500°C), and eventually disappeared (600–800°C). Compared to the synthetic goethite, natural goethite has low crystallinity and small

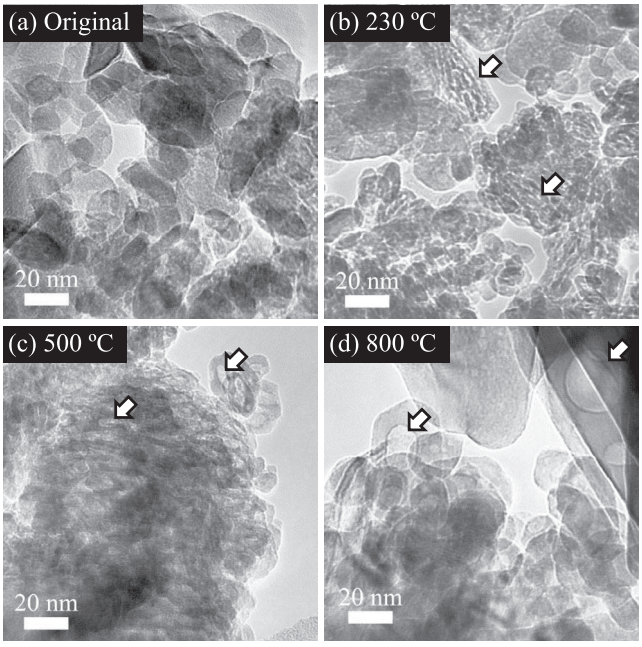

Fig. 10. TEM images of natural goethite; (a) original, (b) heated to 230°C, (c) heated to 500°C, and (d) heated to 800°C. Arrows indicate pore generation in the particles.

primary particle size of under 100 nm.

(2) The original natural goethite before dehydration had 4 nm pores as cracks, and these cracks remained even after heating to 800°C. Thus, it was found that the pore structure not only depended on the decomposition temperature but also on the initial state of goethite including its structures.

(3) The optimum dehydration temperature for higher surface area and pore volume was found to be 250 and 350°C for the synthetic and natural goethite, respectively.

Acknowledgment

The analysis of BET was performed with Autosorb 6AG at the OPEN FACILITY, Hokkaido University Sousei Hall. The TEM observation was conducted at Hokkaido University, supported by the "Nanotechnology Platform" Program of the Ministry of Education, Culture, Sports, Science, and Technology of Japan (MEXT).

REFERENCES

1) U. Schwertmann and R. M. Cornell: Iron Oxides in the Laboratory, Wiley, Germany, (2000).
2) R. M. Cornell and U. Schwertmann: The Iron Oxides, Wiley-VCH Verlag GmbH & Co. KGaA, Germany, (2004), i.
3) H. Liu, T. Chen and R. L. Frost: *Chemosphere*, **103** (2014), 1.
4) J. M. D. Coey: Iron in Soils and Clay Minerals, eds. by J. W. Stucki, *et al.* Springer, Netherlands, (1988), 397.
5) Y. Hata, H. Purwanto, S. Hosokai, J.-i. Hayashi, Y. Kashiwaya and T. Akiyama: *Energy Fuels*, **23** (2009), 1128.
6) T. Murakami, T. Nishimura and E. Kasai: *ISIJ Int.*, **49** (2009), 1686.
7) K. Miura, K. Miyabayashi, M. Kawanari and R. Ashida: *ISIJ Int.*, **51** (2011), 1234.
8) S. Hosokai, K. Matsui, N. Okinaka, K.-i. Ohno, M. Shimizu and T. Akiyama: *Energy Fuels*, **26** (2012), 7274.
9) A. N. Rozhan, R. B. Cahyono, N. Yasuda, T. Nomura, S. Hosokai and T. Akiyama: *Energy Fuels*, **26** (2012), 3196.
10) A. N. Rozhan, R. B. Cahyono, N. Yasuda, T. Nomura, S. Hosokai, H. Purwanto and T. Akiyama: *Energy Fuels*, **26** (2012), 7340.
11) R. B. Cahyono, A. N. Rozhan, N. Yasuda, T. Nomura, H. Purwanto and T. Akiyama: *Energy Fuels*, **27** (2013), 2687.
12) R. B. Cahyono, G. Saito, N. Yasuda, T. Nomura and T. Akiyama: *Energy Fuels*, **28** (2014), 2129.
13) R. B. Cahyono, N. Yasuda, T. Nomura and T. Akiyama: *Fuel Process. Technol.*, **119** (2014), 272.
14) R. B. Cahyono, N. Yasuda, T. Nomura and T. Akiyama: *ISIJ Int.*, **55** (2015), 428.
15) Y. Mochizuki, N. Tsubouchi and T. Akiyama: *Fuel Process. Technol.*, **138** (2015), 704.
16) T. Nomura, R. Cahyono and T. Akiyama: *J. Sustain. Metall.*, **1** (2015), 115.
17) Y. Mochizuki, M. Nishio, N. Tsubouchi and T. Akiyama: *Fuel Process. Technol.*, **142** (2016), 287.
18) Y. Saito, K. Kawahira, N. Yoshikawa, H. Todoroki and S. Taniguchi: *ISIJ Int.*, **51** (2011), 878.
19) T. Akiyama, R. Takahashi and J.-i. Yagi: *ISIJ Int.*, **31** (1991), 24.
20) T. Akiyama, H. Ohta, R. Takahashi, Y. Waseda and J.-i. Yagi: *ISIJ Int.*, **32** (1992), 829.
21) S. Song, F. Jia and C. Peng: *Surf. Rev. Lett.*, **21** (2014), 1450019.
22) H. Liu, T. Chen, X. Zou, C. Qing and R. L. Frost: *Thermochim. Acta*, **568** (2013), 115.
23) S. Gialanella, F. Girardi, G. Ischia, I. Lonardelli, M. Mattarelli and M. Montagna: *J. Therm. Anal. Calorim.*, **102** (2010), 867.
24) I. Mitov, D. Paneva and B. Kunev: *Thermochim. Acta*, **386** (2002), 179.
25) D. Walter, G. Buxbaum and W. Laqua: *J. Therm. Anal. Calorim.*, **63** (2001), 733.
26) C. Goss: *Mineral. Mag.*, **51** (1987), 437.
27) Y. Kashiwaya and T. Akiyama: *J. Nanomater.*, **2010** (2010), Article ID 235609, 12.
28) B. Minéral: *Bull. Mineral*, **111** (1988), 149.
29) H. Naono, K. Nakai, T. Sueyoshi and H. Yagi: *J. Colloid Interface Sci.*, **120** (1987), 439.
30) F. Watari, P. Delavignette, J. Van Landuty and S. Amelinckx: *J. Solid State Chem.*, **48** (1983), 49.
31) H. Naono and R. Fujiwara: *J. Colloid Interface Sci.*, **73** (1980), 406.
32) F. Watari, J. Van Landuyt, P. Delavignette and S. Amelinckx: *J. Solid State Chem.*, **29** (1979), 137.
33) A. F. Gualtieri and P. Venturelli: *Am. Mineral.*, **84** (1999), 895.
34) M. Francombe and H. Rooksby: *Clay Min. Bull.*, **4** (1959), 1.
35) H. Liu, T. Chen, R. L. Frost, D. Chang, C. Qing and Q. Xie: *J. Colloid Interface Sci.*, **385** (2012), 81.
36) H. D. Ruan, R. L. Frost, J. T. Kloprogge and L. Duong: *Spectrochim. Acta, A*, **58** (2002), 479.
37) T. Ishikawa, H. Yamashita, A. Yasukawa, K. Kandori, T. Nakayama and F. Yuse: *J. Mater. Chem.*, **10** (2000), 543.
38) S. Brunauer, P. H. Emmett and E. Teller: *J. Am. Chem. Soc.*, **60** (1938), 309.
39) U. Schwertmann: *Thermochim. Acta*, **78** (1984), 39.
40) The Structure and Properties of Porous Materials, ed. by D. H. Everett, F. S. Stone, Academic Press, New Yok, (1959).